Voltammetric Determination of Trace Zn(II) in Seawater on a Poly(sodium 4-styrenesulfonate)/Wrinkled Reduced Graphene Oxide Composite Modified Electrode

Journal of The Electrochemical Society, 2020 **167** 046519

Voltammetric Determination of Trace Zn(II) in Seawater on a Poly (sodium 4-styrenesulfonate)/Wrinkled Reduced Graphene Oxide Composite Modified Electrode

Su Ma,[1,2] Hong Wei,[2,3] Dawei Pan,[2,3,4,z] Fei Pan,[2,3] Chenchen Wang,[2,3,4] and Qi Kang[1,z]

[1]*College of Chemistry, Chemical Engineering and Materials Science, Key Laboratory of Molecular and Nano Probes, Ministry of Education, Shandong Provincial Key Laboratory of Clean Production of Fine Chemicals, Shandong Normal University, Jinan 250014, People's Republic of China*
[2]*Key Laboratory of Coastal Environmental Processes and Ecological Remediation, Yantai Institute of Coastal Zone Research, Chinese Academy of Sciences, Yantai 264003, People's Republic of China*
[3]*University of Chinese Academy of Sciences, Beijing 100049, People's Republic of China*
[4]*Center for Ocean Mega-Science, Chinese Academy of Sciences, Qingdao 266071, People's Republic of China*

In this study, a novel poly(sodium 4-styrenesulfonate)/wrinkled reduced graphene oxide composite modified glassy carbon electrode (GCE) was prepared successfully. This electrode was used for sensitive detection of trace Zn(II) in seawater by differential pulse voltammetry (DPV). The morphology and electrochemical property of the modified electrode was characterized using scanning electron microscopy (SEM), energy dispersive spectrometry (EDS), Fourier Transform Infrared (FT-IR) spectroscopy, cyclic voltammetry (CV) and electrochemical impedance spectroscopy (EIS). Results showed that the wrinkled graphene layer formed on the electrode surface could significantly promote the electron-transfer and increase the specific surface area of the electrode. Additionally, the poly(sodium 4-styrenesulfonate) film could also effectively improve the stability of the modified electrode, absorb cations and repel anions on the electrode surface. Under the optimal conditions, the linear response to Zn(II) obtained at the modified electrode, was in the range of 5 to 720 nM with a detection limit of 1.67 nM (S/N = 3). Practical applicability of this modified electrode was successfully tested for the determination of Zn(II) in seawater samples with satisfactory results.
 [DOI: 10.1149/1945-7111/ab7b83]

Manuscript submitted December 30, 2019; revised manuscript received February 12, 2020. Published March 12, 2020.

Zinc (Zn) is an essential micronutrient for marine phytoplankton and a biologically active trace metal for other life forms in the oceans, with a global distribution that is similar to nitrate, phosphate and silicate.[1] It is generally considered essential as a cofactor in many enzymes that are involved in the growth of phytoplankton through CO_2 fixation from the atmosphere.[2] The dissolved Zn constitutes a critical source for the bioaccumulation process in organisms because it cannot be destroyed biologically.[3,4] The danger of bio-accumulated Zn is aggravated by its almost indefinite persistence, which poses a potential toxic effect to many aquatic organisms (e.g., hypoxia in gill tissue).[5]

Therefore, it is important to set up a reliable and sensitive method for accurately detecting Zn(II) in the oceans. A variety of methods such as atomic absorption spectrometry (AAS),[6,7] inductively coupled plasma mass spectrometry (ICP-MS),[8–10] inductively coupled plasma atomic emission spectrometry (ICP-AES),[11,12] fluorimetry and ultraviolet-visible spectrophotometry (UV),[13–16] and spectrophotometry[17,18] have been developed and become well established for the determination of zinc. However, these methods are fairly time-consuming, costly and require bulky devices. Comparatively, the benefits like reasonably low cost, short analysis time, non-requirement of prior separation, inherent miniaturization and portability, make stripping voltammetry a prominent method in the field of electrochemical analytical chemistry.[19] Conventionally, mercury electrodes have been employed for heavy-metal detection, as not only does it have a high hydrogen over-voltage, a high repeatability and an easily regenerated surface, but can also form diluted amalgams to prevent the formation of intermetallic compounds.[20,21] However, high toxicity and the risk of its contamination are detrimental to the use of mercury electrodes.[22] Over the past decades, bismuth electrode has been introduced to replace mercury electrode.[23–25] However, bismuth itself, as a heavy-metal element, still has certain toxicity.[26] In recent times, some new modified electrodes were used to detect Zn(II), such as screen-printed carbon electrode modified with bismuth and gold nanoparticles,[27] tin-bismuth alloy,[19] and indium-bismuth nanofilm.[28] But none of them left out bismuth. Therefore, it is essential to find a substance comparable to bismuth for zinc detection.

During recent years, polymer membranes have attracted great attention because their good stability and reproducibility.[29] Membranes such as poly(1,8-diaminonaphthalene),[30] poly(p-aminobenzene sulfonic acid),[31] and polypyrrole[32] have been the favored ones. In this work, Poly(sodium 4-styrenesulfonate) (PSS) was used, and it being a kind of surfactant, can form an orderly membrane, similar to the biofilms formed by lipids in organisms.[33] It can also be bound to the surface of graphene through the π-bonds on the aromatic ring and grapheme.[34] The negatively charged head of PSS can absorb cations and repel anions. Compared to other sulfonic acid series, PSS has very low toxicity and high water solubility. Reduced graphene oxide (rGO) is typically obtained by the chemical/electrochemical reduction of graphene oxide (GO). Because rGO has a high theoretical surface area, it has been used frequently to improve the performance of electrochemical sensors.[35] In recent years, three-dimensional (3D) graphene has been reported.[36] 3D graphene structures exhibit many specific properties such as large surface area and excellent electronic and thermal conductivity.[37] More recently, a new synthetic strategy for preparing 3D rGO by electrochemical reduction of the graphene oxide was proposed.[38] This method exhibits several advantages, such as quick reaction, simplicity and low cost.

In this study, a PSS/wrinkled rGO composite modified electrode was prepared successfully. Wrinkled rGO (W-rGO) with a large specific surface area can provide a large attachment site for PSS, and can also promote electron transfer. PSS can improve the mechanical stability, ion-exchange capacity and anti-interference ability of the electrode. This opens up a new method for the preparation of graphene-based nanocomposites with various functionalities. In addition, the practicality and feasibility of this sensor were verified through the detection of Zn(II) in real seawater samples.

Experimental

Chemicals and solutions.—A standard stock solution of Zn(II) was purchased from Acros Organics (USA). Graphene oxide was

[z]E-mail: dwpan@yic.ac.cn; kangqi@sdnu.edu.cn

purchased from Nanjing XFNANO Materials Tech Co., Ltd. Lithium perchlorate and Poly(sodium 4-styrenesulfonate) were supplied by Alading. All the chemicals were of analytical grade and used without further purification. Deionized water (18.2 MΩ cm specific resistance), obtained from Pall Cascada laboratory water system (USA), was used throughout the experience. Unless stated otherwise, the electrochemical experiments were carried out in 0.1 M acetate buffer (pH 5.0).

Apparatus.—All electrochemical experiments were performed an electrochemical workstation (CHI 660D, CH Instruments, Inc., Shanghai, China) using a conventional three-electrode cell. A glassy-carbon electrode (3 mm in diameter, Chenhua instruments, Shanghai, China) was used as the working electrode, with Ag/AgCl and a platinum foil serving as the reference and counter electrodes, respectively. Scanning electron microscopy (SEM, Hitachi S-4800, Japan) and Fourier transform infrared spectrometry (FT-IR, Nicolet iS50, USA) were used to observe the morphology of the nanomaterials. Comparative testing was done using ICP-MS (ELAN DRC, Perkin Elmer Instruments, USA).

Preparation of PSS/W-rGO modified electrode.—Prior to modification, the GC electrode was thoroughly polished with aqueous slurries of 0.3 μm and 0.05 μm alumina powder, and then sonicated for 3 min each in ethanol and water respectively. PSS/W-rGO was synthesized via a two-step procedure. Initially, the GC electrode was immersed in 1.0 mg ml^{-1} GO containing 0.1 M lithium perchlorate aqueous solution, to electrochemically deposit GO with constant potential at −1.2 V for 200 s.[39] Then the W-rGO modified electrode was rinsed with ultrapure water thoroughly. PSS were decorated on W-rGO modified electrode surface by cyclic voltammetry (scan rate of 0.1 V s^{-1}). The electrode cycling was carried out in the range of −1.4 V to −0.6 V in 0.2 mM PSS for 10 cycles. Then the as-obtained PSS/W-rGO/GCE was washed carefully with deionized water and subsequently dried at room temperature. For comparison purpose, W-rGO and PSS coated GCE were prepared with the same process.

Electrochemical analysis procedure.—Unless stated otherwise, all the experimentations were carried out in the 0.1 M acetate buffer (pH 5.0). Differential pulse voltammetry (DPV) scans over the potential range of −1.3 V to 0.8 V were recorded by using the following parameters: amplitude of 0.05 V, pulse width of 0.2 s, pulse period of 0.5 s, and an equilibrium time period of 2 s. Prior to each cycle, the electrode was cleaned for 100 s at −0.1 V with stirring.

Preparation of real samples.—Seawater samples were collected from Sishili Bay (the North Yellow Sea, Shandong Province, China). The treatment for sample preparation was done as follows: all the seawater samples were filtered (using 0.45 μm membrane filters) into acid-cleaned polyethylene bottles and stored in Teflon bottles at 4 °C before analysis. Prior to detection, the samples of seawater were acidified with adequate amount of HNO_3 and H_2O_2 to adjust the pH of water samples at less than 2.0. Finally the samples were digested in quartz tubes using a 500 W UV lamp (Metrohm MVA-UV 705, Switzerland).

Results and Discussion

Characteristics of PSS/W-rGO modified electrode.—SEM, EDS and FT-IR spectra were used to illustrate the characteristics of the modified electrodes. Figures 1a and 1b showed the morphology of rGO and W-rGO modified electrode, respectively. Compared with the slightly folded film-like rGO, a fractured and wrinkled paper-like structure could be observed on the W-rGO/GCE (Fig. 1b) surface which clearly indicated the formation of W-rGO nanosheets on the surface of electrodes. The crumpled nature of W-rGO was very much beneficial in preserving the large surface area of the electrode throughout the cycles. Figure 1c displays the obvious flat surface of PSS-modified GCE. When PSS was decorated onto the W-rGO/GCE (Fig. 1d), the thickness of the layered structure of W-rGO nanosheets increased significantly, demonstrating that the polymer was indeed coated on its surface. The perfectly covered structure of PSS/W-rGO composite film indicated that there existed a strong interfacial interaction between the polymer and W-rGO components. The rGO has a π-conjugated structure with a highly hydrophobic surface, which could interact with PSS through both hydrophobic interaction as well as the π-π conjugation between the benzene ring structures of PSS.[40,41] Additionally, the electro-deposition of PSS under applied potential might urge PSS to combine with W-rGO. Therefore, on the surface of W-rGO, PSS can form stable three-dimensional nanocomposites, which further increases the physical adsorption of electroactive substances on the surface of electrodes.

The EDS pattern of PSS/W-rGO/GCE as shown in Fig. 1e, also indicated that C, O, Na and S were the major elements present in the composites. C and O might have come from W-rGO. The peak of Na and S revealed the existence of PSS. Thus, PSS was proven to conjugate on the surface of W-rGO.

In Fig. 2, the FT-IR spectrum of GO displays characteristic absorption peaks of oxygen-containing functional groups, including the O–H stretching vibrations at 3420.91 cm^{-1}, the C=O stretching vibration at 1730.11 cm^{-1}, the C–O–C (epoxy groups bending) at 1230.22 cm^{-1} and the C–O bending vibration at 995.23 cm^{-1}, respectively. In the FT-IR spectrum of PSS/W-rGO, the peaks of oxide groups (C=O, C–O, C–O–C) practically vanished. Two new peaks at 1522.95 cm^{-1} and 1384.34 cm^{-1} can be ascribed to the skeletal vibrations of the graphene sheets. The other new peaks at 1164.27 cm^{-1} and 1115.99 cm^{-1} were assigned to the C–S bond. The peaks at 1034.42 cm^{-1} and 899.09 cm^{-1} corresponded to S–OH.[42] These results indicated that a significant part of the oxygen-containing functional groups had been removed while the PSS polymer got attached to the surface of W-rGO.

Electrochemical behavior of different modified electrode.—The voltammetric behaviors of various electrodes were studies in 0.1 M KCl solution containing 5 mM $Fe(CN)_6^{3-/4-}$. As shown in Fig. 3, a pair of well-defined redox peaks was discovered in bare GCE (curve a), which was due to the reversible one-electron redox behavior of ferricyanide. The anodic peak current (Ip) was 60.6 μA. After modifying PSS on the GCE (curve b), a pair of significantly decreased redox peaks were exhibited (Ip = 51.7 μA), suggesting that PSS polymer membrane acted as a block layer and hampered the charge transfer at the interface. Compared with the PSS-modified electrode (curve b), the redox peak currents were obviously increased on the W-rGO-modified GC electrode (curve c) (Ip = 125.0 μA). A pair of the obvious redox peak (Ip = 93.9 μA) were also obtained at PSS/W-rGO/GCE (curve d). The W-rGO had higher density of edge-plane-like defects that could offer some favorable active sites for accelerating the charge transfer.

The electroactive areas of modified electrodes were estimated according to the Randles-Sevcik equation:

$$Ip = 2.69 \times 10^5 A D^{1/2} n^{3/2} v^{1/2} C \quad [1]$$

Where Ip was the anodic peak current (A). A was the surface area of the electrode (cm^2). D was the diffusion coefficient. n was the electron transfer number. C was the concentration of $K_3Fe(CN)_6$ (mM) and v was the scan rate (V s^{-1}). According to the literature,[43,44] in 5 mM $K_3Fe(CN)_6$ solution containing 0.1 M KCl, n equaled 1 and D was 6.1 × 10^{-6} cm^2 s^{-1}. Thus, the active surface areas of PSS/W-rGO/GCE, W-rGO/GCE, PSS/GCE and GCE were calculated and equaled 0.13 cm^2, 0.17 cm^2, 0.07 cm^2 and 0.08 cm^2, respectively. The results indicated that the existence of W-rGO could increase of the active surface of the electrode obviously. The active surface areas of PSS/W-rGO/GCE was almost twice than that of GCE and PSS/GCE.

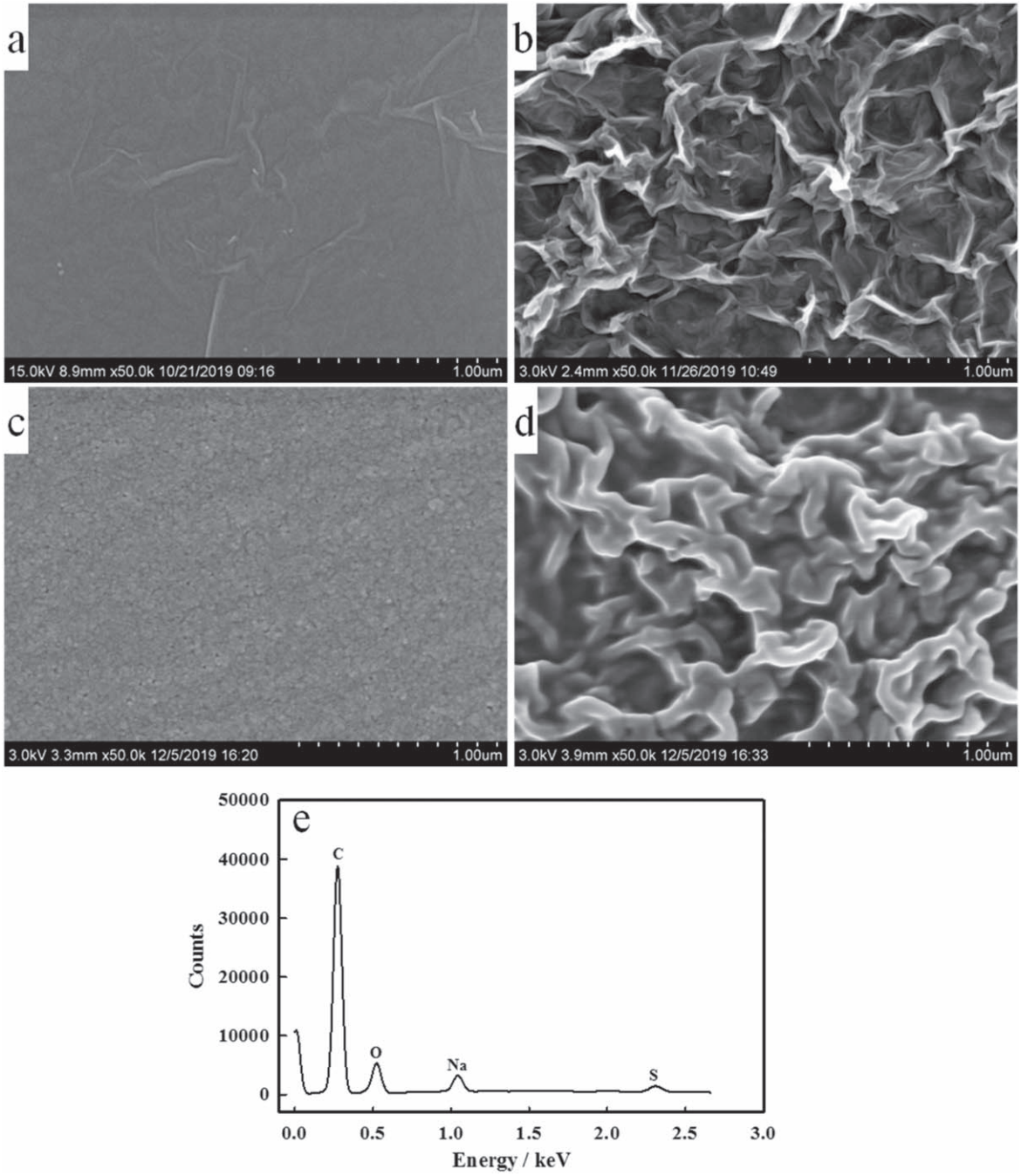

Figure 1. SEM images of rGO/GCE (a), W-rGO/GCE (b), PSS/GCE (c), PSS/W-rGO/GCE (d) and EDS of PSS/W-rGO/GCE (e).

The electron transfer kinetics were further explored with electrochemical impedance spectrum (EIS) analysis. The semicircular diameter of EIS was taken as the charge transfer resistance (R_{et}) that depended on the electrolyte interface and the dielectric features of the material present on the electrode. The Nyquist diagrams of different electrodes were obtained from 5 mM $Fe(CN)_6^{3-/4-}$ a solution containing 0.1 M KCl. As shown in Fig. 4, the bare GCE (curve a) exhibited a very low electron-transfer resistance ($R_{ct} = 680$ Ω). After the GCE was modified by W-rGO (curve b), the value of Rct was obtained as 220 Ω, which was typical of a diffusion-limited process. In the PSS-modified electrode, the Rct increased to 850 Ω (curve c), implying that the PSS introduced a barrier to the electronic transfer. The reason for this may be that the PSS film with negative charge has a larger repulsion effect on the probe ion $[Fe(CN)_6]^{3-/4-}$. The electrostatic absorption would be occurred between the positively charged redox probes ($[Ru(NH_3)_6]^{3+/2+}$) on the surface of PSS-modified electrode, which had been reported in literatures.[45–47] On the PSS/W-rGO-modified GC electrode (curve d), an obvious semicircle with an Rct of 320 Ω was obtained. This may be due to the fact that W-rGO has higher conductivity and larger specific surface area, which promotes charge transfer. W-rGO in PSS film plays an important role similar to that of conducting electron transfer tunnel.[29] Such a phenomenon has also been reported in case of other polymers/rGO modified electrodes,[31,48] demonstrating that W-rGO played an important role as an "electron-conducting tunnel," and could efficiently improve the electron-transfer rate of the electrode.

The DPV response of as-prepared electrodes was obtained in 0.1 M acetate buffer solution (pH 5.0) containing 230 nM Zn(II). As shown in Fig. 5, curves a, b, c and d were the conditions without Zn

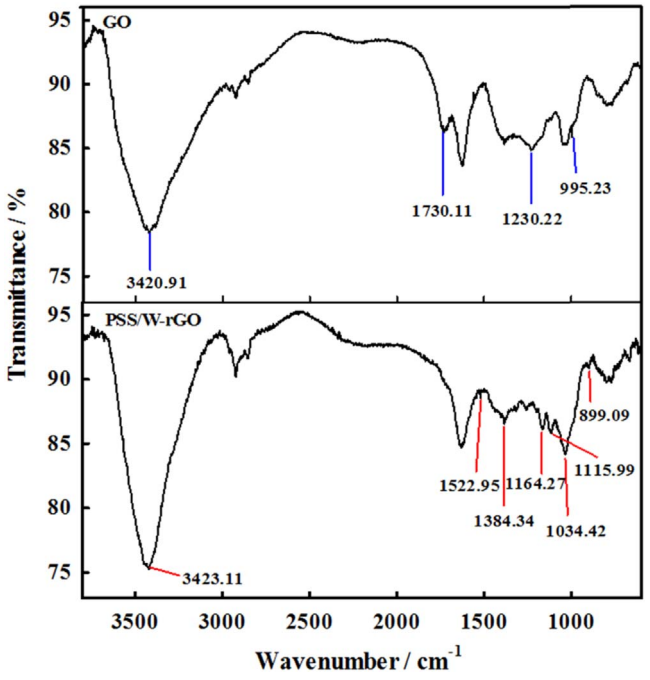

Figure 2. FT-IR spectra of GO, PSS/W-rGO.

(II). There was no response from Zn(II) on the bare glassy-carbon electrode (curve e) under low concentrations of Zn(II). At W-rGO/GCE, a small anodic peak near −1.15 V was observed in presence of Zn(II) (curve f) compared with that in absence of Zn(II) (curve b). There was also a small peak with the use of PSS/GCE (curve g). This may be because of the negatively charged PSS which facilitates the non-faradaic pre-concentration of Zn(II). The response current at the target modified electrode (curve h) was larger than the sum of the individual currents at the W-rGO and PSS modified electrodes, indicating that the modified electrode has a good detection affinity for zinc. This enhancement can be explained by two reasons. Firstly, W-rGO can offer a large surface area for PSS, which can synergistically improve the anodic current response of Zn(II). Secondly, the high conductivity of PSS/W-rGO nanocomposite membrane efficiently accelerates electron-transfer between the analyte and the electrode surface.

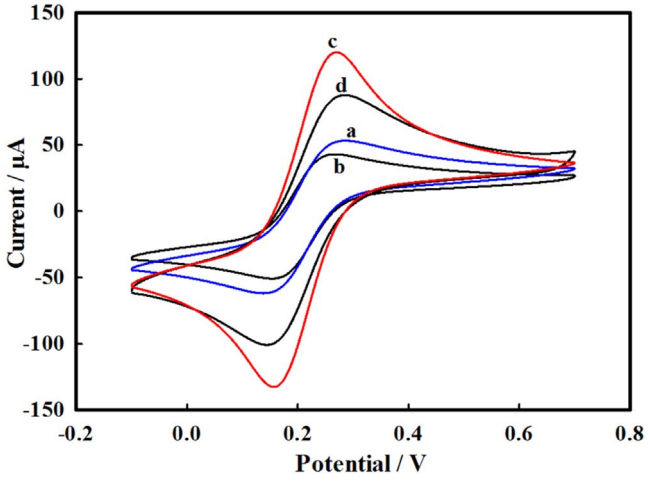

Figure 3. Cyclic voltammograms of 5 mM $Fe(CN)_6^{3-/4-}$ in 0.1 M KCl solution at bare GCE (a), PSS/GCE (b), W-rGO/GCE (c), and PSS/W-rGO/GCE (d).

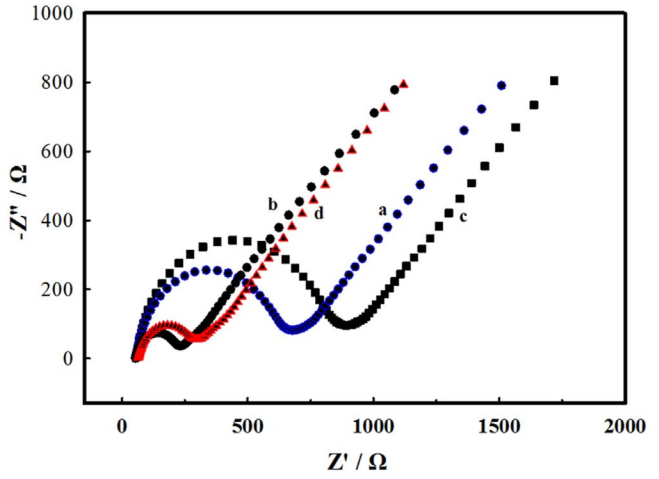

Figure 4. Nyquist plots of bare GCE (a), W-rGO/GCE (b), PSS/GCE (c), and PSS/W-rGO/GCE (d) in 0.1 M KCl solutions containing 5 mM $Fe(CN)_6^{3-/4-}$.

Optimization for Zn(II) determination using PSS/W-rGO/GCE.—To obtain the best response current, the DPV responses of 230 nM Zn(II) in acetate buffer solution was used as a "model" to investigate the different experimental parameters.

The effect of 0.1 M acetate buffer solution in the pH range of 4.0–6.0 on the dissolution peak of Zn(II) was further explored. As shown in Fig. 6a, the maximum current was obtained at pH 5.0 and the peak current decreased when the pH values went below 5.0. This probably resulted from the effect of hydrogen dissolution which caused high background current from the initial scan that partly overlapped the stripping peak current. Moreover, the current decreased as the pH values went above 5.0, which was a consequence of a low background current, and a lower response current simultaneously. As a result, pH 5.0 was selected as the optimum experimental condition.

The stripping response of Zn(II) was closely related to the thickness of the polymer membrane. The relationship between the scan rate and scan cycles with the stripping peak of Zn(II) was shown in Figs. 6b and 6c. Results established that the maximum stripping peak was observed when the scan cycle and scan rate were fixed at 10 cycles and 100 mV s^{-1}. The reason can be attributed to the competition between two effects: The coatings could cause the

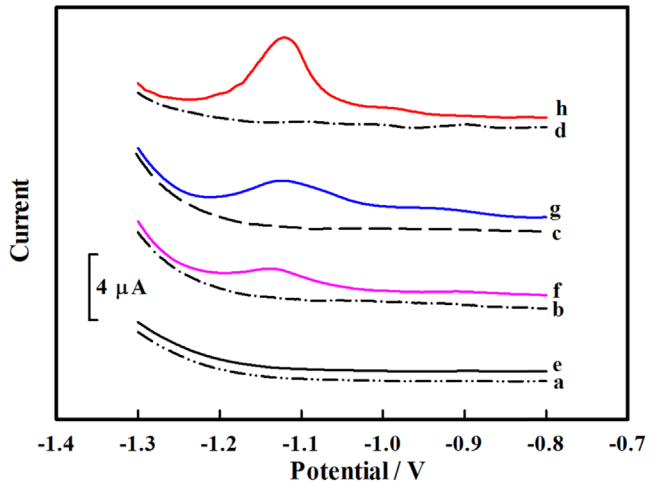

Figure 5. DPV response curves in 0.1 M acetate buffer (pH 5.0) without (a)–(d) and with (e)–(h) 230 nM Zn(II) at bare GCE (a), (e), W-rGO/GCE (b), (f), PSS/GCE (c), (g), and PSS/W-rGO/GCE (d), (h). Parameters: amplitude of 0.05 V, pulse width of 0.2 s, pulse period of 0.5 s, and an equilibrium time period of 2 s.

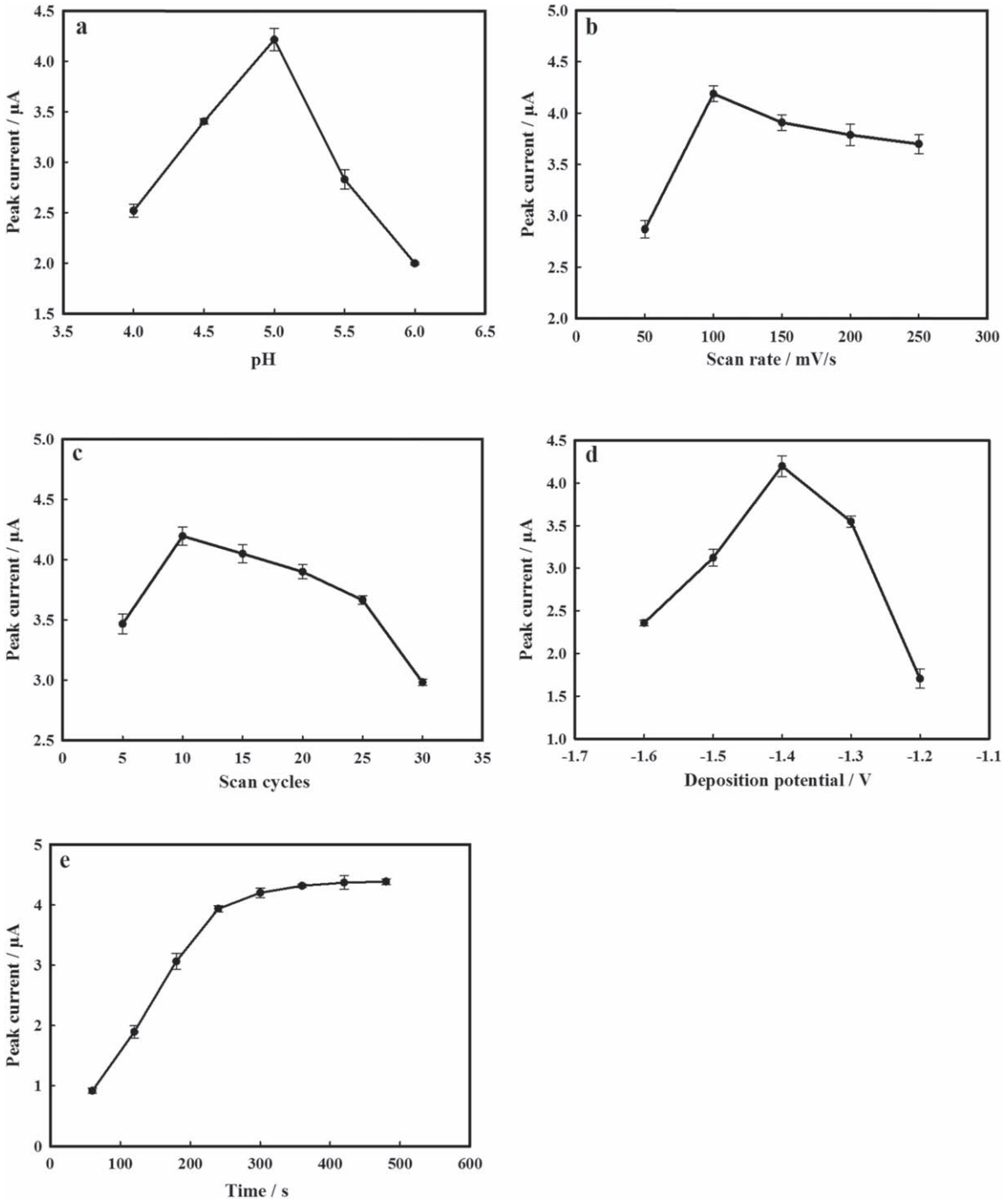

Figure 6. Effects of the pH values (a) of acetate buffer solution, scan rate (b) and the scan cycles (c) of 0.2 mM PSS, deposition potential (d) and the deposition time (e) on the DPV peak current for 230 nM Zn(II) in 0.1 M acetate buffer solution at the PSS/W-rGO/GCE. n = 3.

enhancement of cation exchange activity and the thickness of polymers could inhibit the reduction of conductivity.

Figure 6d shows the influence of the deposition potential of Zn(II) at the modified electrode surface. Increased peak current was observed when the potential gradually increased from −1.6 to −1.4 V, and this was due to the greater reduction of available Zn(II) ions. However, the peak currents decreased gradually as the deposition potential became more negative, which was a result of hydrogen evolution. As shown in Fig. 6e, the peak currents increased almost linearly with the increase in deposition time from 60–300 s, and then tended to increase slowly. Therefore, −1.4 V and 300 s were chosen as the preferred parameters for the subsequent DPV method for Zn(II) detection.

Analytical performance in Zn(II) detection.—Under the optimized experimental conditions, the calibration curve for Zn(II) determination using PSS/W-rGO/GCE by DPV method was shown in Fig. 7. It can be seen that the stripping voltammograms correspond to the different concentrations of Zn(II). In the concentration range from 5 to 720 nM, the peak currents exhibit a favorably linear relationship, and the linear regression equation can be expressed as follows: $Ip = 0.0184\ C + 0.1397$ ($R^2 = 0.998$), with the theoretical LOD of 1.67 nM (S/N = 3). In addition, as shown in Table I, a comparison of Zn(II) determination by various electrochemical and other analytical methods has been listed, indicating that the proposed method in this work offers an acceptable

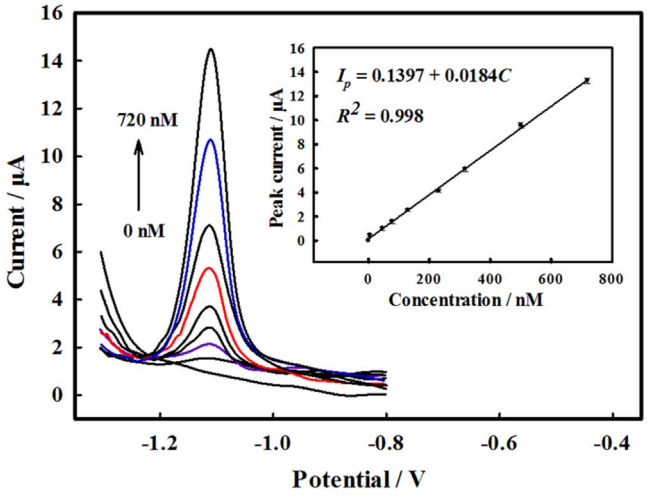

Figure 7. DPV voltammograms of the PSS/W-rGO/GCE in 0.1 M acetate buffer (pH 5.0) containing different Zn(II) concentrations (5 to 720 nM). Parameters: amplitude of 0.05 V, a pulse width of 0.2 s, pulse period of 0.5 s, and an equilibrium time period of 2 s. Left: The calibration curve for Zn(II) detection (n = 3).

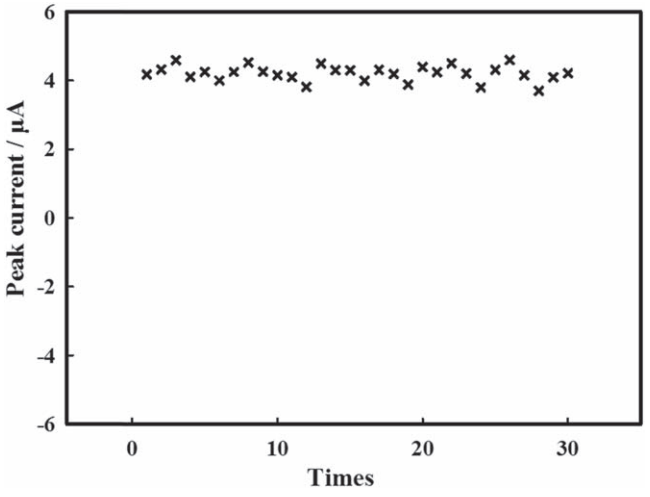

Figure 8. Repeatability of the modified-electrode (PSS/W-rGO/GCE) for 30 times measurements in 0.1 M acetate buffer solution (pH 5.0) containing 230 nM Zn(II).

sensitivity, lower detection limit and a wider linear range for Zn(II) determination.

Reproducibility, repeatability, and interference.—The reproducibility of PSS/W-rGO modified GCE was evaluated by using six independently modified electrodes and the solution with 230 nM Zn (II), which produced a relative standard deviation (RSD) of 5.7%. This result indicated that the PSS/W-rGO/GCE did not produce any observable difference between stripping peaks of the prepared electrodes. In addition, the repeatability of the PSS/W-rGO modified-GCE was tested in the same solution. The modified electrode was repeatedly used for 30 times, as shown in Fig. 8, the stripping peak current almost remained unchanged and the RSD was 5.4%, revealing acceptable repeatability in continuous determination.

Under the experimental conditions used for the determination of 230 nM Zn(II), NH_4^+, K^+, Mg^{2+}, Ca^{2+}, Cu^{2+}, Pb^{2+}, and Cd^{2+}, were selected as interfering ions owing to their wide availability in natural waters. In the standardized experiment, the concentration of interfering ions was adjusted to 100 times higher than that of Zn(II) ions. The outcome of these experiments showed that the cations (NH_4^+, K^+, Mg^{2+}, Ca^{2+}) had no obvious interference on the Zn(II) stripping signal of the sensor. The high selectivity of the present modified electrode resulted from two reasons. One was the existence of negative charge of PSS, which could avoid the interference of anions. Another was the use of stripping method. The different ions had different dissolution peak potential. There was no interference unless the stripping peak potential was overlapped. Nonetheless, Cu^{2+}, Pb^{2+}, and Cd^{2+} were found to have a huge influence on the stripping response of Zn(II). This was possibly because of the competition between these interfering ions deposited on the working electrode. Concentration of Cu(II) being 5 times and that of Pb(II) and Cd(II) being 20 times higher than the concentration of Zn(II) ions were the respective tolerance limits for the electrode to be able to detect Zn(II). This interference phenomenon has also been reported previously.[49,50] According to the deposition potential of Cu and Zn, it was easier to electrochemically deposited of Cu than that of Zn and easy to form the Zn–Cu intermetallic compounds. However, when Ga(III) was added, the effect of Cu(II) on Zn(II) could be eliminated.[51,52] The total dissolved concentration of Cu(II) in seawater was lower than 5 times the concentration of Zn(II), so the Zn(II) in seawater could be detected directly.

Detection of Zn(II) in seawater samples.—To evaluate the practical applicability of the PSS/W-rGO modified electrode, the target modified-electrode was employed to detect Zn(II) in seawater samples. The comparison of results obtained for determination of Zn(II) in seawater by this method and ICP-MS is listed in Table II. These results indicated that the method in this

Table I. Comparison of the analytical performance of the proposed electrochemical sensor with other reported methods for Zn(II) determination.

Methods[a)]	Electrode/agents[b)]	Linear range (nM)	Detecting limit (nM)	References
AAS	HNO_3/H_2O_2	7.6×10^3–4.5×10^4	8.5×10^2	6
ICP-MS	HNO_3	—	4.8×10^1	10
ICP-MS	HNO_3/H_2O_2	2.4×10^3–6.1×10^5	1.5×10^2	9
fluorometry	Cu–In–S QDs	0–8.0×10^2	3.0×10^1	14
spectrophotometry	4-(2-pyridylazo)resorcinol	1.0×10^3–1.0×10^4	—	17
DPASV	Bi/AuNPs/SPCE	—	7.6×10^{-1}	27
SWASV	Bi/LCP	4.6–1.1×10^4	1.2	50
SWV	SnBiE	5.0×10^2–2.5×10^4	5.0×10^1	19
DPV	PSS/W-rGO/GCE	5.0–7.2×10^2	1.7	Present work

a) Methods: AAS, atomic absorption spectrometry; ICP-MS, inductively coupled plasma mass spectrometry; DPASV, differential pulse anodic stripping voltammetry; SWASV, Square wave anodic stripping voltammetry; SWV, square wave voltammetry; DPV, differential pulse voltammetry. b) Electrode/reagents: Cu–In–S QDs, Cu–In–S quantum dots; Bi/AuNPs/SPCE, bismuth film/gold nanoparticles/screen-printed carbon electrode; Bi/LCP, bismuth film/liquid crystal polymer; SnBiE, tin-bismuth alloy; Bi@In/GCE, indium doped bismuth nanofilm/glassy carbon electrode; PSS/W-rGO/GCE, poly(sodium 4-styrenesulfonate)/wrinkled reduced graphene oxide/glassy carbon electrode.

Table II. Determination of Zn(II) in real seawater samples by the proposed and ICP-MS methods.

Samples	Zn(II) added (nM)	Mean[a)] ± SD	Recovery (%)	ICP-MS (nM)
Sample 1	0	295.0		296.2
	30.0	325.0 ± 2.7	100.0	
	50.0	375.1 ± 2.9	100.2	
Sample 2	0	315.9		316.9
	30.0	345.5 ± 2.9	98.7	
	50.0	395.7 ± 3.1	100.4	
Sample 3	0	305.2		304.1
	30.0	335.1 ± 4.0	99.7	
	50.0	385.2 ± 2.4	100.2	
Sample 4	0	390.5		289.8
	30.0	419.9 ± 3.8	98.0	
	50.0	469.0 ± 2.1	98.2	
Sample 5	0	286.9		287.6
	30.0	317.2 ± 3.1	101.0	
	50.0	366.9 ± 3.5	99.4	

a) Mean is calculated from three determinations.

work is reliable, consistent and suitable for analysis of Zn(II) in seawater.

Conclusion

In summary, a novel, low-priced, and effective PSS/W-rGO modified electrode was successfully fabricated for sensitive detection of Zn(II) in real seawater samples. Compared to other modified electrodes, the synthesis method used in this work was relatively uncomplicated and easily accessible. The modified-electrode in this work had a low detection limit, good reproducibility, and repeatability. Additionally, due to the presence of a conductive W-rGO layer, the electrode exhibited excellent electrochemical activity and accelerated charge-transfer rate. The PSS component provides high adsorption ability and good antifouling performance, which makes the modified electrode an effective option for sensitive determination of Zn(II) in seawater.

Acknowledgments

This work was financially supported by the National Natural Science Foundation of China (21874083), the Natural Science Foundation of Shandong Province (ZR2018MB029), Original Innovation Project of Chinese Academy of Sciences (ZDBS-LY-DQC009) and the Key Research and Development Plan of Yantai City (2017ZH096).

ORCID

Dawei Pan https://orcid.org/0000-0002-6166-9707

References

1. T. M. Conway and S. G. John, *Global Biogeochem. Cycles*, **28**, 1111 (2014).
2. S. G. John, J. Helgoe, and E. Townsend, *Mar. Chem.*, **201**, 256 (2018).
3. S. S. Murugan, R. Karuppasamy, K. Poongodi, and S. Puvaneswari, *Tur. J. Fish. Aqust. Sci.*, **8**, 55 (2008), http://www.trjfas.org/abstract.php?lang=en&id=589.
4. K. W. Bruland, *Earth Planet. Sci. Lett.*, **47**, 176 (1980).
5. C. Hogstrand, R. W. Wilson, D. Polar, and C. M. Wood, *J. Exp. Biol.*, **186**, 55 (1994), https://jeb.biologists.org/content/186/1/55.
6. C. C. Pereira, A. O. de Souza, E. Q. Oreste, M. A. Vieira, and A. S. Ribeiro, *Food Chem.*, **240**, 959 (2018).
7. S. Popović, A. Pantelić, Ž. Milovanović, J. Milinkov, and M. Vidović, *Anal. Lett.*, **50**, 2619 (2017).
8. M. L. Astolfi, E. Marconi, C. Protano, M. Vitali, E. Schiavi, P. Mastromarino, and S. Canepari, *Anal. Chim. Acta*, **1040**, 49 (2018).
9. A. Londonio, E. Morzán, and P. Smichowski, *Food Chem.*, **284**, 149 (2019).
10. G. Xing, M. R. Sardar, B. Lin, and J. M. Lin, *Talanta*, **204**, 50 (2019).
11. M. Mitić, A. Pavlović, S. Tošić, P. Mašković, D. Kostić, S. Mitić, G. Kocić, and J. Mašković, *Microchem. J.*, **141**, 197 (2018).
12. P. Y. Sharanov, D. S. Volkov, and N. V. Alov, *Anal. Methods*, **11**, 3750 (2019).
13. K. Huang, R. Dai, W. Deng, S. Guo, H. Deng, Y. Wei, F. Zhou, Y. Long, J. Li, and X. Yuan, *Sens. Actuators, B*, **255**, 1631 (2018).
14. M. Mou, Y. Wu, H. Zou, J. Dong, S. Wu, Z. Yan, and S. Liao, *Sens. Actuators, B*, **284**, 265 (2019).
15. K. Rout, A. K. Manna, M. Sahu, and G. K. Patra, *Inorg. Chim. Acta*, **486**, 733 (2019).
16. Y. Wang, S. Lao, W. Ding, Z. Zhang, and S. Liu, *Sens. Actuators, B*, **284**, 186 (2019).
17. C. E. Säbel, J. L. Shepherd, and S. Siemann, *Anal. Biochem.*, **391**, 74 (2009).
18. F. Zhou, C. Li, H. Zhu, and Y. Li, *Optik*, **182**, 58 (2019).
19. D. Pan, L. Zhang, T. Yin, and W. Qin, *Microchimi. Acta*, **177**, 59 (2012).
20. A. Economou and P. R. Fielden, *Analyst*, **128**, 205 (2003).
21. Ø. Mikkelsen and K. H. Schrøder, *Analyst*, **125**, 2163 (2000).
22. E. Gustafsson, *Water Air Soil Pollut.*, **80**, 99 (1995).
23. J. Ping, J. Wu, Y. Ying, M. Wang, G. Liu, and M. Zhang, *J. Agric. Food Chem.*, **59**, 4418 (2011).
24. J. Wang, J. Lu, S. B. Hocevar, P. A. Farias, and B. Ogorevc, *Anal. Chem.*, **72**, 3218 (2000).
25. Z. Wang, G. Liu, L. Zhang, and H. Wang, *Int. J. Electrochem. Sci.*, **7**, 12326 (2012), http://www.electrochemsci.org/papers/vol7/71212326.pdf.
26. W. Serfontein and R. Mekel, *Res. Commun. Chem. Pathol. Pharmacol.*, **26**, 391 (1979), https://europepmc.org/article/med/392661.
27. Z. Lu, J. Zhang, W. Dai, X. Lin, J. Ye, and J. Ye, *Microchim. Acta*, **184**, 4731 (2017).
28. R. Ouyang, L. Xu, H. Wen, P. Cao, P. Jia, T. Lei, X. Zhou, M. Tie, X. Fu, and Y. Zhao, *Int. J. Electrochem. Sci.*, **13**, 1423 (2018).
29. Y. Zhang, Y. Cai, and S. Su, *Anal. Biochem.*, **350**, 285 (2006).
30. K. M. Hassan, G. M. Elhaddad, and M. AbdelAzzem, *Microchim. Acta*, **186**, 440 (2019).
31. Z. Wang, H. Wang, Z. Zhang, X. Yang, and G. Liu, *Electrochim. Acta*, **120**, 140 (2014).
32. K. Ma, A. Sinha, X. Dang, H. Zhao, and A. Liu, *J. Electrochem. Soc.*, **166**, B147 (2019).
33. W. Cheng, G. Jin, and Y. Zhang, *Sens, Actuators, B*, **114**, 40 (2006).
34. G. Wang, B. Wang, J. Park, Y. Wang, B. Sun, and J. Yao, *Carbon*, **47**, 3242 (2009).
35. K. Dutta and S. Panda, *J. Electrochem. Soc.*, **166**, B1335 (2019).
36. P. Xu, J. Yang, K. Wang, Z. Zhou, and P. Shen, *Chin. Sci. Bull.*, **57**, 2948 (2012).
37. L. Shi, Z. Chu, Y. Liu, W. Jin, and N. Xu, *Adv. Funct. Mater.*, **24**, 7032 (2014).
38. C. Li and G. Shi, *Nanoscale*, **4**, 5549 (2012).
39. K. Sheng, Y. Sun, C. Li, W. Yuan, and G. Shi, *Sci. Rep.*, **2**, 247 (2012).
40. G. Wang, J. Park, Y. Wang, B. Sun, and J. Yao, *Carbon*, **47**, 3242 (2009).
41. L. Wang, R. Yang, J. Li, L. Qu, and P. B. Harrington, *Talanta*, **196**, 309 (2019).
42. Y. Fan, Y. Liu, Q. Cai, Y. Liu, and J. Zhang, *Synth. Met.*, **162**, 1815 (2012).
43. K. P. Prathish, M. M. Barsan, D. Geng, X. Sun, and C. M. A. Brett, *Microchim. Acta*, **114**, 533 (2013).
44. J. Kudr, L. Richtera, L. Nejdl, K. Xhaxhiu, P. Vitek, B. Rutkay-Nedecky, D. Hynek, P. Kopel, V. Adam, and R. Kizek, *Materials*, **9**, 31 (2016).
45. D. M. Fernandes, M. E. Ghica, A. M. V. Cavaleiro, and C. M. A. Brett, *Electrochim. Acta*, **56**, 7940 (2011).
46. N. Gu, D. Wei, L. Niu, and A. Ivaska, *Electrochim. Acta*, **51**, 6038 (2006).
47. G. Panzarasa, M. DÜbner, V. Pifferi, G. Soliveri, and C. Padeste, *J. Mater. Chem. C*, 1 (2013).
48. S. Yu, X. Cao, and M. Yu, *Microchem. J.*, **103**, 125 (2012).
49. J. Meng, F. Li, L. Luo, X. Wang, and M. Xiao, *Monatshefte für Chemie-Chemical Monthly*, **145**, 161 (2014).
50. N. Wang, E. Kanhere, A. G. P. Kottapalli, J. Miao, and M. S. Triantafyllou, *Microchim. Acta*, **184**, 3007 (2017).
51. A. Królicka and A. Bobrowski, *Electrochim. Acta*, **187**, 224 (2016).
52. C. M. A. Brett, M. B. Q. Garcia, and J. L. F. C. Lima, *Anal. Chim. Acta*, **339**, 167 (1997).